

Article

Effects of Precipitant and pH on Coprecipitation of Nanosized Co-Cr-V Alloy Powders

Xiaoyu Chen ^{1,2}, Yongxia Li ¹, Lan Huang ^{1,3}, Dan Zou ¹, Enxi Wu ¹, Yanjun Liu ¹, Yuanyan Xie ¹, Rui Yao ^{1,2}, Songyi Liao ^{1,2}, Guangrong Wang ^{1,2} and Feng Zheng ^{1,2,3,*} 

¹ Hunan Boyun-Dongfang Powder Metallurgy Co., Ltd., Changsha 410083, China; ChenXY@csu.edu.cn (X.C.); liyongxia1959@hnboyun.com.cn (Y.L.); lhuang@csu.edu.cn (L.H.); zdlyl@189.cn (D.Z.); wuenxi@163.com (E.W.); bydflyj@163.com (Y.L.); mingjian004@126.com (Y.X.); yaorui205@csu.edu.cn (R.Y.); songyiliao@csu.edu.cn (S.L.); g3504251992@163.com (G.W.)

² School of Materials Science and Engineering, Central South University, Changsha 410083, China

³ State Key Laboratory of Powder Metallurgy, Central South University, Changsha 410083, China

* Correspondence: fzheng@csu.edu.cn; Tel.: +86-731-88876179; Fax: +86-731-88879692

Received: 8 August 2017; Accepted: 4 September 2017; Published: 21 September 2017

Abstract: Nanosized Co-Cr-V alloy powders were synthesized via coprecipitation method. Effects of precipitants ((NH₄)₂C₂O₄·H₂O and Na₂CO₃) and pH were investigated by X-ray diffraction (XRD), Zeta potential analyzer, thermogravimetry-differential scanning calorimetry (TG-DSC), inductively coupled plasma-atomic emission spectrometry (ICP-AES) and scanning electron microscopy (SEM). Co-Cr-V alloy powders were consisted of major face-centered cubic Co (fcc Co) and minor hexagonal close-packed Co (hcp Co). Grain sizes of precursors and Co-Cr-V alloy powders were increased with pH value (7–10) within the ranges of 3~39 and 39~66 nm, respectively. Rod-like or granular Co-Cr-V alloy particles were assembled by interconnected nanograins. At pH = 7, Na₂CO₃ precipitant was found to be beneficial to maintain the desirable composition of Co-Cr-V powders. It was also found that lower pH favors the maintenance of pre-designed composition, while grain coarsens at higher pH. Effects of variation for precipitant and pH on the morphology and composition of Co-Cr-V alloy powder were discussed in detail and relevant mechanism was further proposed.

Keywords: Co-Cr-V alloy; morphology coarsening; coprecipitation; precursor; nanosize

1. Introduction

Possessing many unique properties such as impressive fatigue and creep strength at high temperature [1,2], good biocompatibility [3] and excellent resistance to oxidation [4], corrosion [2,5], and sulfidation [2,5], cobalt-based alloys are widely used as wear resistant, magnetic, high strength materials and catalysts [6–10]. Effects of alloying elements such as Ni, Cr, Ta, W, Nb, and Mo have been studied by numerous researchers over the last half century.

Addition of 20~30 at % Cr into cobalt metal can provide superior oxidation and hot corrosion resistance [11]. Co-Cr based alloys have also found utilization as suitable magnetic recording and biomedical applications [12,13]. Similarly, Co-V system is a potential candidate of ultra-high density recording media due to separation between ferromagnetic hcp phase and non-magnetic hcp phase [14]. According to isothermal sections of Co-Cr-V ternary phase diagrams at 25, 800, 1000, 1100, 1150, and 1200 °C [15], adding 0~10 at % of both Cr and V into cobalt metal simultaneously may also lead to phase separation as that observed in Co-V system. These findings suggested that Co-Cr-V ternary alloys should be of great promise as either structural or magnetic recording materials.

Due to various favorable nanosize-related effects, extensive efforts have been made recently to explore the dependence of material properties on composition and size of cobalt-based alloy nanoparticles mainly in binary systems with different morphologies such as nanowires [16,17],

nanotubes [18] and nanorings [2], etc. A variety of synthesis methods, including coprecipitation route [19], hydrothermal/solvothermal [20,21], polyolprocess [22], electrodeposition [18], double composite template approach [23], mechanical alloying [24], chemical vapor deposition [25], and nonaqueous ethylene glycol refluxing [26], have been explored in those works. Coprecipitation route has been proved to be one of the feasible ways to produce highly dispersed, well inter-mixed and uniform cobalt-based alloy nanoparticles [27]. However, despite high industrial and scientific importance for nanosize Co-Cr-V alloy particles stated above, no such work associated with their synthesis, to the best of our knowledge, has been reported up to date.

The objective of the present paper is to study the effects of precipitant and pH on material properties of Co-Cr-V nanoparticles derived from coprecipitation route. Crystal structure, grain size, phase content, morphology and thermal behavior of precursors and final products will be examined and discussed in details.

2. Materials and Methods

2.1. Materials

All chemicals used here are of analytical grade produced by Xilong Chemical Co. Ltd. (Shantou, China) without further purification. $\text{CoCl}_2 \cdot 6\text{H}_2\text{O}$, $\text{CrCl}_3 \cdot 6\text{H}_2\text{O}$ and NH_4VO_3 were chosen and acted as sources of Co, Cr and V, respectively. Two different precipitants, i.e., $(\text{NH}_4)_2\text{C}_2\text{O}_4 \cdot \text{H}_2\text{O}$ and Na_2CO_3 , were employed to compare their effects on physicochemical properties of Co-Cr-V alloy powders. Aqueous ammonia was added to adjust pH value and PVP was employed as dispersant.

2.2. Synthesis

Typical synthesis of Co-Cr-V alloy powders (shown in Figure 1) was performed in two basic stages: (I) preparation of precursors by wet chemical coprecipitation method, and (II) heat treatment of precursors to obtain Co-Cr-V alloy powders.

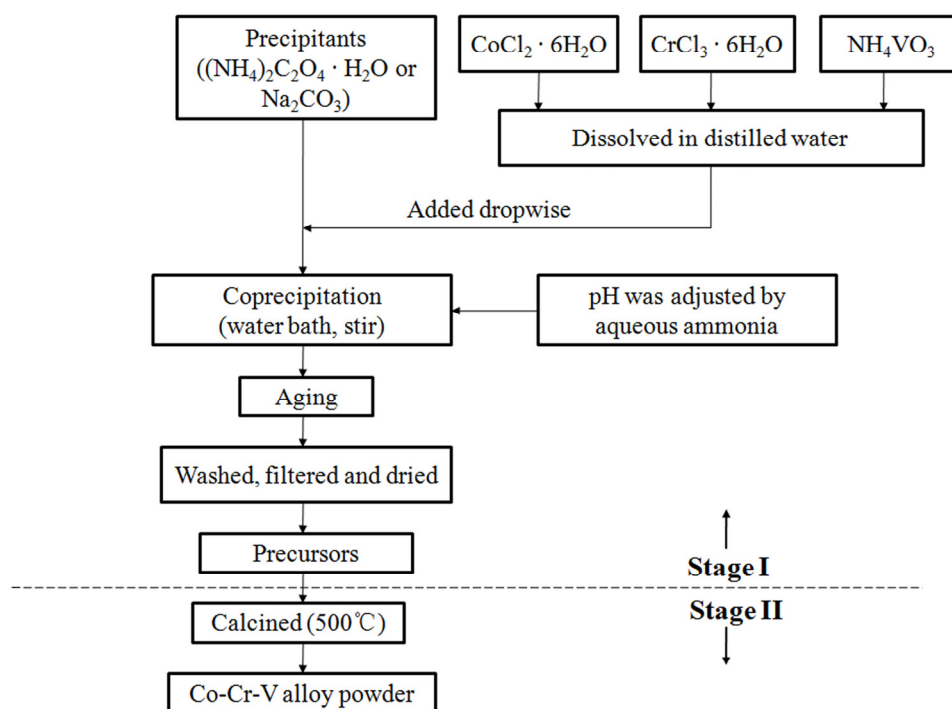


Figure 1. Flow chart of synthesis.

There are six steps involved in Stage I:

- (1) $\text{CoCl}_2 \cdot 6\text{H}_2\text{O}$, $\text{CrCl}_3 \cdot 6\text{H}_2\text{O}$ and NH_4VO_3 were dissolved in distilled water at molar ratio of Co:Cr:V = 8:1:1 to prepare mixed salt solution of 0.5 mol/L with addition of 2 mol % PVP as dispersant.
- (2) The above solution was equally divided into six parts for later use.
- (3) Each part (of the solution) was dropped (4 mL/min) into aqueous solution of precipitant (1 mol/L $(\text{NH}_4)_2\text{C}_2\text{O}_4 \cdot \text{H}_2\text{O}$ or Na_2CO_3 solution) at designated pH value via constant pressure funnel. Excessive precipitant by 20 mol % was used to ensure fully precipitation of metallic ions.
- (4) Coprecipitation (i.e., Step 3) was thermostated in water bath at 50 °C for 1 h with continuous magnetic stirring. pH value of the solution was monitored (by pH meter) and maintained as constant by adding aqueous ammonia.
- (5) Solution with precipitates after coprecipitation was aged in open air for 12 h at room temperature.
- (6) As-prepared precipitates were washed with deionized water by filtrating (filtrates were collected for subsequent testing), dried at 80 °C overnight to obtain precursors denoted with PO for oxalates and PC for basic carbonates.

Stage II: Both oxalate and basic carbonate precursors were kept at 500 °C (heating rate of 5 °C/min) for 3 h in hydrogen atmosphere, then cooled down to room temperature to get Co-Cr-V alloy powders, and denoted as AO and AC, accordingly.

All samples including precursors and alloy powders were named according to their synthesis parameters, as presented in Table 1.

Table 1. Synthesis conditions and names of samples.

Samples		Parameters of Synthesis	
Precursor	Alloy Powder	Precipitant	pH Value
PO1	AO1	$(\text{NH}_4)_2\text{C}_2\text{O}_4 \cdot \text{H}_2\text{O}$	7
PO2	AO2		9
PO3	AO3		10
PC1	AC1	Na_2CO_3	7
PC2	AC2		9
PC3	AC3		10

2.3. Characterization

Phases of precursors and alloy powders were determined by X-ray diffraction (XRD) analysis using an X-ray diffractometer (D/Max 2500, Rigaku, Japan) with $\text{CuK}\alpha$ radiation ($\lambda = 0.154060 \text{ \AA}$). Grain size was calculated through Scherrer Equation by the strongest peak:

$$d = \frac{K\lambda}{\beta_{1/2} \cos \theta} \quad (1)$$

where d is the mean crystallite diameter, the X-ray wave length, K the Scherrer constant (0.89), $1/2$ the full-width at half-maximum (FWHM) of the main diffraction peak of crystalline phase and the diffraction angle. Relative phase content of alloy powders and their lattice parameters were obtained by Rietveld method using Jade[®] 6.0 program. Zeta potentials at different pH were measured by Zeta potential analyzer (Zetasizer Nano ZS, Malvern, UK). Thermogravimetry (TG) and differential scanning calorimetry (DSC) curves of precursors were measured and recorded by DSC200F3 Maia (NETZSCH, Bavaria, Germany) between 35 and 700 °C at heating rate of 10 °C/min in argon atmosphere. Residual concentrations of metallic ions in filtrates were determined by inductively coupled plasma-atomic emission spectrometry (ICP-AES, PS-6, Baird, Milwaukee, WI, USA). Morphology of all powder samples were examined by scanning electron microscopy (SEM, Quanta-200, FEI, Hillsboro, OR, USA).

3. Results and Discussion

3.1. XRD Analysis

XRD patterns of precursors and their thermally decomposed products (alloy powders) are presented in Figure 2a–d. All diffraction peaks for samples PO1–PO3 were corresponding to cobalt oxalate ($\text{CoC}_2\text{O}_4 \cdot 2\text{H}_2\text{O}$, JCPDS No. 25-0250), and those for samples PC1–PC3 were indexed as basic cobalt carbonate ($\text{Co}(\text{CO}_3)_{0.5}(\text{OH}) \cdot 0.11\text{H}_2\text{O}$, JCPDS No. 48-0083). No secondary phase was detectable here. All products heated at 500 °C with flowing hydrogen from either oxalate (AO1–AO3) or basic carbonate precursors (AC1–AC3) yielded a mixture of two types of cobalt phases, i.e., fcc Co (JCPDS No. 89-7093) and hcp Co (JCPDS No. 89-7094). No peak can be assigned to either Cr- or V-containing phase.

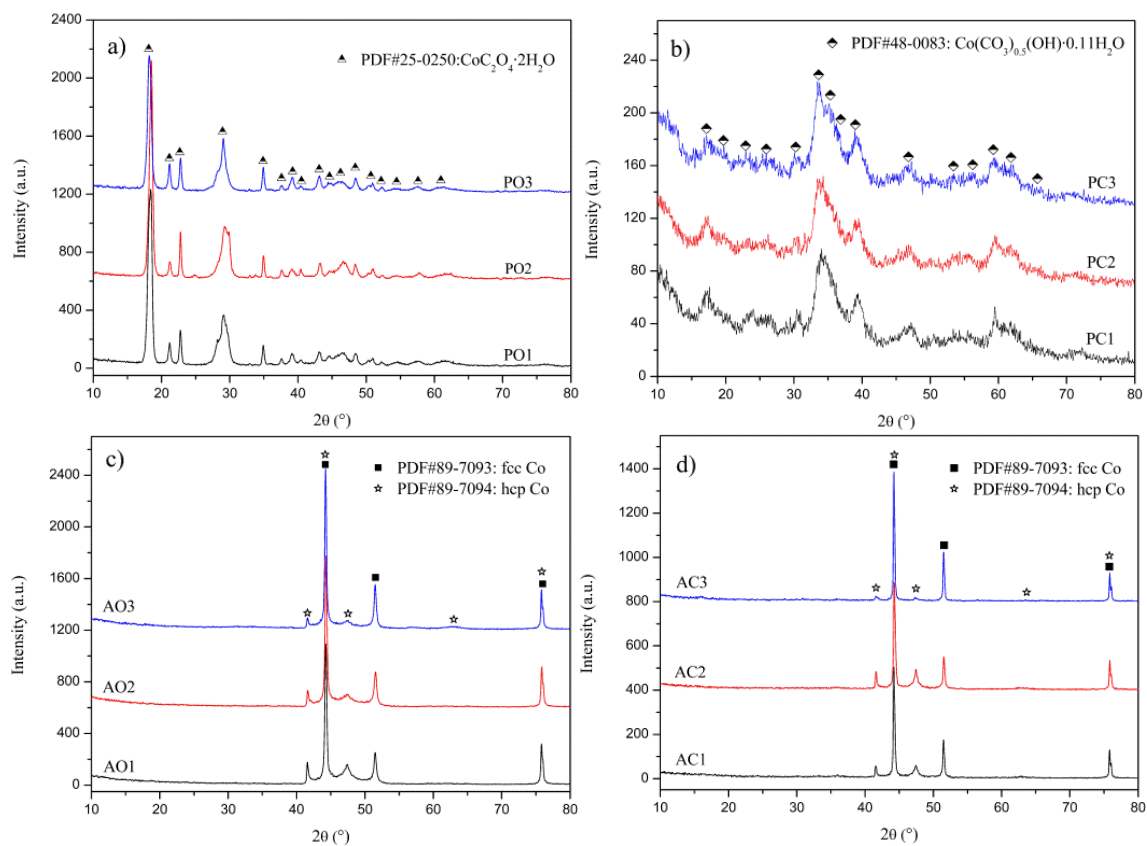


Figure 2. XRD patterns of : (a,b) precursors; and (c,d) Co-Cr-V alloy powders.

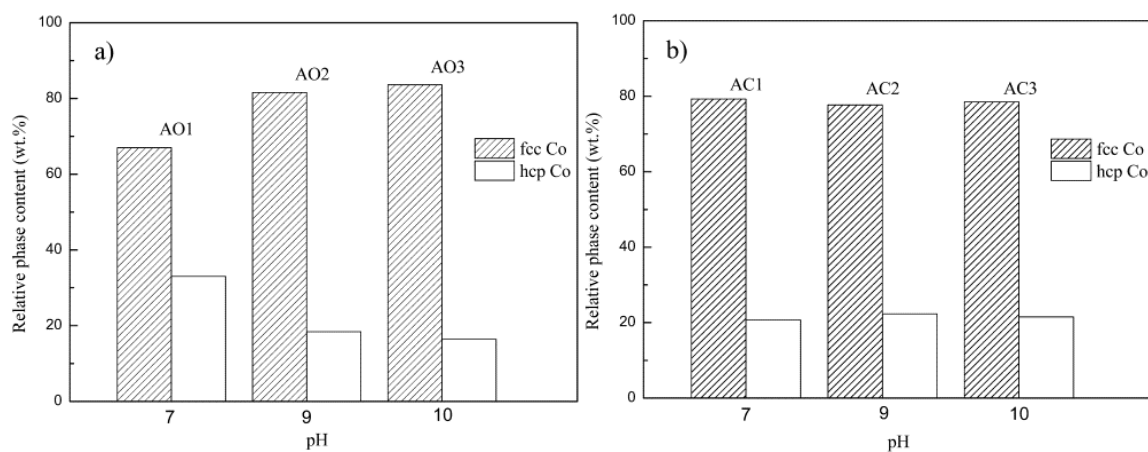
Lattice parameters of alloy powders were obtained by Rietveld analysis and listed in Table 2. We noted lattice distortions for both fcc Co and hcp Co phases in all samples by comparing their lattice parameters with those of powder diffraction files (PDFs) inside Jade[®] 6.0. Considering atomic radius of Co (1.26 Å), Cr (1.27 Å) and V (1.35 Å), substitution of Co by Cr and especially V will necessarily lead to expansion of crystal lattice. Our data listed in Table 2 showed apparent expansion along three dimensions for fcc Co phase and c-axis for hcp Co phase, indicating that Cr and/or V should have dissolved into Co matrix. Moreover, composition of alloy powders confirmed the existence of both Cr and V together with Co (detailed discussion will be provided later in Section 3.3), which lead us to believe and conclude that Co have been partially substituted by Cr and V to form solid solution, which is in agreement with Co-Cr-V ternary phase diagrams [15]. These also implied that, during aqueous reaction stage, both Cr and V ions have simultaneously precipitated with those of Co to form single-phased precursor.

Table 2. Lattice parameters of alloy powders.

Samples	Lattice Parameters (Å)		
	fcc	hcp	
	A = b = c	a = b	c
AO1	3.5493 ± 0.0010	2.5066 ± 0.0008	4.0853 ± 0.0007
AO2	3.5482 ± 0.0003	2.5068 ± 0.0009	4.0886 ± 0.0009
AO3	3.5463 ± 0.0009	2.5071 ± 0.0012	4.0924 ± 0.0017
AC1	3.5448 ± 0.0007	2.5076 ± 0.0012	4.0989 ± 0.0029
AC2	3.5455 ± 0.0001	2.5063 ± 0.0015	4.0913 ± 0.0036
AC3	3.5461 ± 0.0006	2.5071 ± 0.0010	4.0929 ± 0.0023
JCPDS No.89-7093 (fcc Co)	3.5442	-	-
JCPDS No.89-7094 (hcp Co)	-	2.5074	4.0699

Considering the fact that there was no oxidation-reduction reaction occurred during coprecipitation, it is then believed that Cr and V ions should maintain their original valence states of 3⁺ and 5⁺ in precipitates, respectively. To maintain charge neutrality, some vacancies must form and exist in precipitates. In other words, precipitates could be expressed as (Co_{x1}Cr_{x2}V_{x3}□_{x4})C₂O₄·2H₂O and (Co_{y1}Cr_{y2}V_{y3}□_{y4})(CO₃)_{0.5}(OH)·0.11H₂O for oxalate and basic carbonate precursors, accordingly, with □ representing for vacancy. Detailed calculation of the two sets of variables, x₁–x₄ and y₁–y₄, will be discussed in Section 3.3.

Relative phase contents of both fcc Co and hcp Co in alloy powders were calculated from XRD patterns, as given in Figure 3a,b. It turned out that fcc Co phase is dominant for all samples, indicating that fcc Co phase is stable at room temperature here. This is, interestingly, different from knowledge for conventional coarse-grain Co metal, whereas the stable phase is hcp Co [28]. The reason for stabilization of fcc Co at room temperature will be discussed later.

**Figure 3.** Relative phase content of fcc Co and hcp Co in samples of: (a) AO1–AO3; and (b) AC1–AC3.

Average grain sizes of all samples calculated from Scherrer equation using full-width at half-maximum of the strongest diffraction peak (202) for oxalate, (221) for basic carbonate precursors, (111) for fcc Co, and (101) for hcp Co are tabulated in Table 3. Results show that average grain sizes of oxalate and basic carbonate precursors increased with pH value and ranged 13–39 and 3–6 nm, respectively.

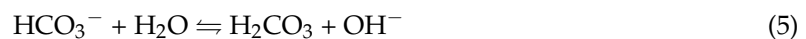
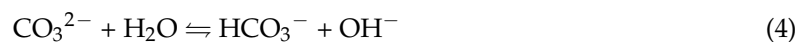
Table 3. Grain sizes of precursors and alloy powders.

Precursors	Grain Size (nm)	Alloy Powders	Grain Size (nm)	
			fcc Co	hcp Co
PO1	13	AO1	40	44
PO2	15	AO2	41	46
PO3	39	AO3	48	65
PC1	3	AC1	39	46
PC2	4	AC2	59	66
PC3	6	AC3	43	58

There is no universal mechanism in the literature for the effects of pH variation on grain growth for salt solution. However, it has been well documented that grain growth and particles agglomeration are controlled effectively by change of pH value of precipitating medium [29–31]. Nucleation and grain growth in aqueous solution are affected by the presence of different types of ions, their concentrations and interactions as well as intrinsic properties of precipitates. In our case, samples were prepared in solutions with different pH value where concentrations of H^+ and OH^- varied from each other. Solution at higher pH yields higher concentration of OH^- , which will drive ionic equilibrium of $C_2O_4^{2-}$ or CO_3^{2-} (Equations (2)–(5)) to shift towards left, resulting in higher content of $C_2O_4^{2-}$ or CO_3^{2-} .



or



On the one hand, once there are larger amount of $C_2O_4^{2-}$ or CO_3^{2-} in the solution system at higher pH value, the frequency of collision among ions of reactants will be increased and thereby boost grain growth, leading to increase of grain size with pH value under low supersaturation (metal salts were added dropwise). On the other hand, we supposed that surfaces of precipitates would attain stronger negative charges at higher pH due to absorption of $C_2O_4^{2-}$ or CO_3^{2-} , resulting in larger potential difference between surfaces of precipitates and diffuse layers in solution. To quantitatively analyze potential difference of particles during reaction to examine this hypothesis, Zeta potentials (characterization of potential difference between surface of solid particles and diffuse layers [32]) were measured, as given in Figure 4. In Figure 4, we can see that absolute values of Zeta potential (0.27~10.9 and 9.18~13.3 mV for oxalate and basic carbonate precursors, respectively) did increase with pH, supporting our hypothesis. With larger potential difference between surfaces of precipitates and diffuse layers in solution, diffusion fluxes of metallic ions (Co, Cr and V ions here) and thus grain growth of precipitates would be increased greatly. These allow us to believe that potential difference between particle surface and diffuse layers should also be responsible for grain coarsening.

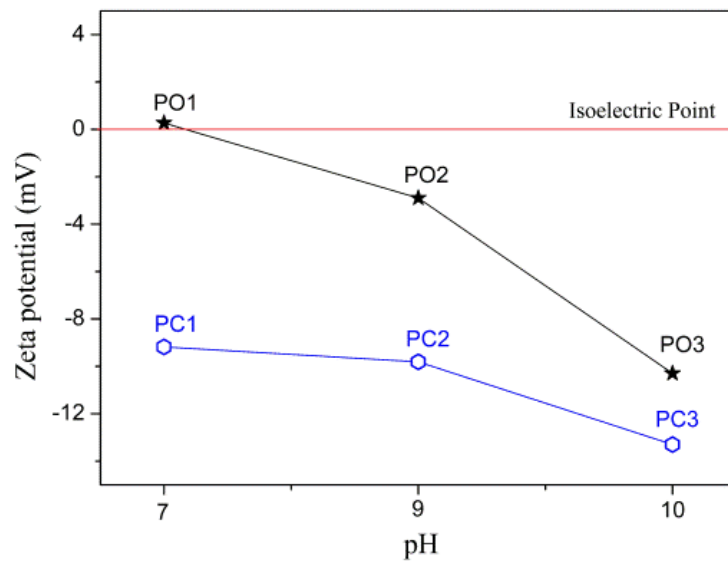


Figure 4. Zeta potential of filtrates as function of pH value.

All alloy powder samples are in nanosize scale (≤ 100 nm) with average grain size ranging from 40 to 60 nm. The tendency of grain size varying with pH is generally consistent with that of precursors. Usually, coarse Co will undergo phase transition of fcc \rightarrow hcp (around 420 °C) at cooling from high temperature. However, it is suggested that fcc Co could be stabilized and retained to room temperature instead of going through transition to hcp structure if its grain size is smaller than critical size (usually nanometer scale), [33,34]. The exact value of that critical size may depend on experimental conditions, e.g. 20 nm [35] or 35 nm [36]. Considering our case, where most alloy powders are in the lattice structure of fcc Co phase rather than hcp one at room temperature, conclusions could be made such that: (1) the exact critical sizes to retain fcc Co structure here are larger than those obtained in [35,36]; and (2) for each of our samples, most grains are smaller than the critical size, leading to the absence of allotropic transition of fcc Co \rightarrow hcp Co during cooling to room temperature.

3.2. Thermal Behavior of Precursors

Typical TG and DSC curves of precursors PO1 and PC1 in argon atmosphere are presented in Figure 5a,b, respectively.

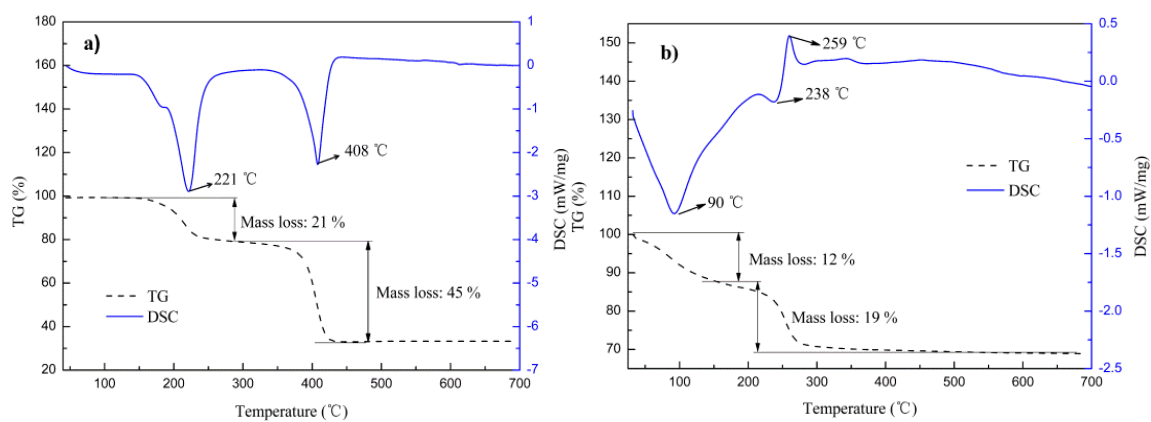
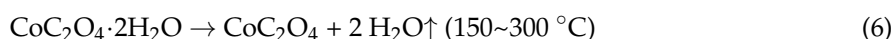


Figure 5. TG and DSC curves for samples of: (a) PO1; and (b) PC1.

For oxalate precursor PO1, two main endothermic peaks took place around 221 and 408 °C accompanied by mass losses of roughly 21% and 45% within 150~300 °C and 300~450 °C, respectively.

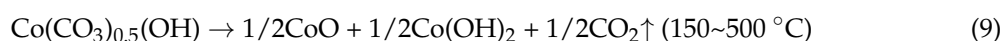
The first mass loss of 21% is close to that (of 20%) caused by loss of crystal water, while the second loss of 45% agrees approximately with expected value of 48% calculated from decomposition of pure CoC_2O_4 to Co. According to XRD analysis, PO1 should be a complex compound $(\text{Co}_{x_1}\text{Cr}_{x_2}\text{V}_{x_3}\square_{x_4})\text{C}_2\text{O}_4 \cdot 2\text{H}_2\text{O}$ rather than $\text{CoC}_2\text{O}_4 \cdot 2\text{H}_2\text{O}$. The mass variation resulted from substitution of Co by Cr and V could be subtle because of: (1) similar atomic mass of Cr (52.00 amu), V (50.94 amu) and Co (58.93 amu); and (2) relatively low content of Cr and V. Hence, the second mass change can be attributed to complete decomposition from $(\text{Co}_{x_1}\text{Cr}_{x_2}\text{V}_{x_3}\square_{x_4})\text{C}_2\text{O}_4 \cdot 2\text{H}_2\text{O}$ to Co-based alloy accompany by release of CO_2 . Corresponding phase transition referred to these two mass losses could be described as the following:



For basic carbonate precursor PC1, two mass losses occurred around 80~150 °C and 150~500 °C, respectively. The first mass loss of 12% is ascribed to dehydration of surface-absorbed water and some structural water with one observable endothermic peak. For $\text{Co}(\text{CO}_3)_{0.5}(\text{OH})$, it is chemically identical to $1/2[\text{CoCO}_3 \cdot \text{Co}(\text{OH})_2]$, both CoCO_3 and $\text{Co}(\text{OH})_2$ can be thermally decomposed into CoO with the former occurred around 400 °C and the latter at 1000 °C in air. Hence, we believed that the second mass loss occurred around 150~500 °C in argon due to removal of CO_2 by decarbonation from CoCO_3 to CoO, accompanying mass loss of 19%, which is close to theoretical value of 18% from $1/2[\text{CoCO}_3 \cdot \text{Co}(\text{OH})_2]$ changing to $1/2[\text{CoO} \cdot \text{Co}(\text{OH})_2]$. Note, the second mass loss was supposed to be an endothermic process. In addition to one endothermic peak occurred at 238 °C here, however, one exothermic peak appeared at 259 °C. We have then inferred that some intermediate product(s) (multiple oxides, for example) might be formed during phase transition, subjecting to oxidation-reduction reaction through self-catalysis with thermal emission. Phase transition of basic carbonate precursor at heat treatment in argon was therefore given as:



(note: x contains surface-absorbed moisture and some structural water)



In summary, mass losses corresponding to different reaction processes as well as phase evolutions of precursors (PO1 and PC1) have been examined and presented in Table 4.

According to aforementioned thermal and XRD analysis, we believe that basic carbonate precursor is thermally more stable than that of oxalate one, and using of flowing hydrogen is necessary to form pure Co-Cr-V alloy powders.

Table 4. Thermal decomposition analysis for precursors.

Sample	Temperature (°C)	Mass loss (wt %)		Phase Evolution	Thermal Effect
		Exp.	Theor.		
PO1	150~300	21	20	$\text{CoC}_2\text{O}_4 \cdot 2\text{H}_2\text{O} \rightarrow \text{CoC}_2\text{O}_4$	Endoth./221 °C
	300~450	45	48	$\text{CoC}_2\text{O}_4 \rightarrow \text{Co}$	Endoth./408 °C
PC1	80~150	12	/	$\text{Co}(\text{CO}_3)_{0.5}(\text{OH}) \cdot x\text{H}_2\text{O} \rightarrow \text{Co}(\text{CO}_3)_{0.5}(\text{OH})$	Endoth./90 °C
	150~500	19	18	$\text{Co}(\text{CO}_3)_{0.5}(\text{OH}) \rightarrow \text{CoO} + \text{Co}(\text{OH})_2$	Endoth./238 °C partial Exoth./259 °C

3.3. Composition Analysis of Precursors and Co-Cr-V Alloy

Maintaining preset molar ratio of Co, Cr and V (8:1:1) is of vital importance for our final products, i.e., Co-Cr-V alloy powders. Their compositions are closely related to pH value during solution reactions. For our solution system consisting of $\text{Me-NH}_4^+ \cdot \text{NH}_3 \cdot \text{C}_2\text{O}_4^{2-}$ (or CO_3^{2-})- H_2O , diversified coordination reactions would take place besides coprecipitation to consume partial metallic ions to

form soluble metal-ammonia complex $\text{Me}(\text{NH}_3)_n^{x+}$, where n and x represents coordination number and valence of metal, respectively. As a result, not all metallic ions went into precipitates and thereby the actual molar ratio of Co, Cr and V might deviate from preset value of 8:1:1. The level of this deviation depends on solubility of precipitates and stability of soluble complexes which may vary with pH value during reaction [37].

Careful ICP-AES measurement and calculation on residual concentrations of metallic ions in filtrates from coprecipitation process have revealed the yield of each alloying element as well as chemical composition of precursors and Co-Cr-V alloy powders, as shown in Figure 6a,b (with target yield of Co set to be 80% and that of both Cr and V to be 10%) and listed in Table 5.

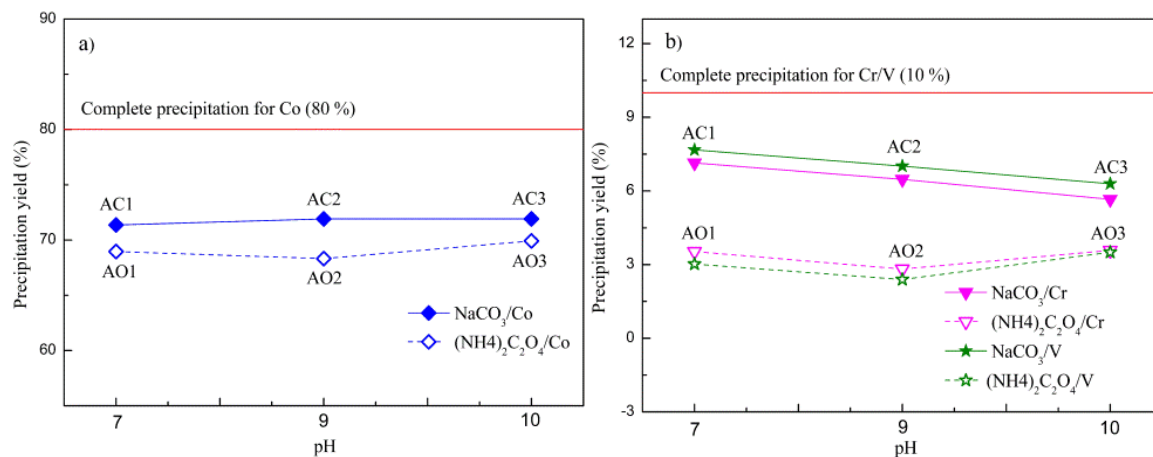


Figure 6. Yields of: (a) Co; and (b) Cr and V as functions of precipitant and pH.

Table 5. Chemical compositions of precursors and Co-Cr-V alloy powders.

Precursor Samples	Calculated Chemical Formula of Precursors	Alloy Samples	Composition of Alloy Powders	Molar Ratio of Co:Cr:V
PO1	$(\text{Co}_{0.84}\text{Cr}_{0.04}\text{V}_{0.04}\square_{0.08})\text{C}_2\text{O}_4 \cdot 2\text{H}_2\text{O}$	AO1	$\text{Co}_{0.91}\text{Cr}_{0.05}\text{V}_{0.04}$	8:0.41:0.35
PO2	$(\text{Co}_{0.87}\text{Cr}_{0.04}\text{V}_{0.03}\square_{0.06})\text{C}_2\text{O}_4 \cdot 2\text{H}_2\text{O}$	AO2	$\text{Co}_{0.93}\text{Cr}_{0.04}\text{V}_{0.03}$	8:0.33:0.28
PO3	$(\text{Co}_{0.84}\text{Cr}_{0.04}\text{V}_{0.04}\square_{0.08})\text{C}_2\text{O}_4 \cdot 2\text{H}_2\text{O}$	AO3	$\text{Co}_{0.91}\text{Cr}_{0.05}\text{V}_{0.04}$	8:0.41:0.40
PC1	$(\text{Co}_{0.71}\text{Cr}_{0.07}\text{V}_{0.07}\square_{0.15})(\text{CO}_3)_{0.5}(\text{OH}) \cdot 0.11\text{H}_2\text{O}$	AC1	$\text{Co}_{0.83}\text{Cr}_{0.08}\text{V}_{0.09}$	8:0.80:0.86
PC2	$(\text{Co}_{0.73}\text{Cr}_{0.06}\text{V}_{0.07}\square_{0.14})(\text{CO}_3)_{0.5}(\text{OH}) \cdot 0.11\text{H}_2\text{O}$	AC2	$\text{Co}_{0.84}\text{Cr}_{0.08}\text{V}_{0.08}$	8:0.72:0.78
PC3	$(\text{Co}_{0.75}\text{Cr}_{0.06}\text{V}_{0.06}\square_{0.13})(\text{CO}_3)_{0.5}(\text{OH}) \cdot 0.11\text{H}_2\text{O}$	AC3	$\text{Co}_{0.86}\text{Cr}_{0.07}\text{V}_{0.07}$	8:0.63:0.70

According to Co-Cr-V alloy composition (see Table 5) and principle of charge neutrality, the two sets of variables, x_1 – x_4 and y_1 – y_4 , mentioned in Section 3.1 have been calculated with detailed chemical formulas for oxalate and basic carbonate precursors presented in Table 5.

As illustrated in Figure 6a,b, for both types of precursors, the yield of Co remained almost constant with pH and closed to target yield of 80% at pH = 7~10. While those of Cr and V appeared to be much lower than target ones and sensitive to pH, especially for oxalate precursors with yields of both Cr and V to be about 3% (target yield of 10%). With respect to basic carbonate precursors, the yields of both Cr and V were decreased with pH and in the range of 6~8%. Chemical composition of resulting alloy powders prepared at pH = 7 (AC1) was $\text{Co}_{0.83}\text{Cr}_{0.08}\text{V}_{0.09}$ with molar ratio of Co, Cr and V to be 8:0.80:0.86, close to predesigned value (8:1:1) than samples obtained at higher pH values. In another word, higher pH values would favor coordination reactions rather than coprecipitation in system containing $\text{Me-NH}_4^+-\text{NH}_3-\text{CO}_3^{2-}-\text{H}_2\text{O}$. Hence, more metallic ions would stay in the solution as part of soluble complexes $\text{Me}(\text{NH}_3)_n^{x+}$, preventing precipitation of Cr and V and causing larger deviation of molar ratio (Co:Cr:V) from preset value. Interestingly, different trend was observed for oxalate precursors such that their yields of Cr and V decreased first and then increased with pH. This is believed to be closely related to the variation of stability of those metal-ammonia complexes, which could only be stable at certain pH range and will dissociate to free metallic ions again under high alkaline condition, resuming precipitation, as was the case for AO3 prepared at pH of 10.

Generally speaking, Na_2CO_3 is a more effective precipitant due to its causing much higher yields of Co, Cr and V than that of $(\text{NH}_4)_2\text{C}_2\text{O}_4 \cdot \text{H}_2\text{O}$. Furthermore, $\text{pH} = 7$ is beneficial to maintain preset composition of Co-Cr-V powders.

3.4. Morphology Analysis

Morphologies of precursors and alloy powders are shown in Figures 7 and 8, respectively. Oxalate precursors (PO1–PO3) are composed of well dispersive rod-like particles with length of 2–10 μm , while basic carbonate precursors (PC1–PC3) appeared as granular agglomerates from fine grains (see Figure 7). The difference in morphologies of those two types of precursors is closely related to different crystal structure of oxalate and basic carbonate molecules [38]. For oxalate precursors, central metal atom was bonded by two $\text{C}_2\text{O}_4^{2-}$ ions to form a planar molecule. Perpendicular to the molecular plane there are two coordinated H_2O molecules by which crystal grain can grow in an elongate way along axial direction, leading to rod-like shapes [39]. For basic carbonate precursors, due to almost equal growing speed along different directions, they then grew into granular shape. Superstructure of Co-Cr-V alloy powders was inherited from their precursors, which can be observable from Figure 8. These alloy powders are in fact formed by a large amount of rather uniform nanoparticles interconnected with each other along original direction of precursors. Formation of new crystallite phase(s) had occurred in situ as such that their relative positions of particles being kept unchanging as those from corresponding precursors. In addition, as indicated in TG-DSC results (Figure 5), there were gaseous H_2O and CO_2 released from precursors during heat treatment, which led to disruption of tightly packed rod-like and granular morphologies and resulted in the formation of architectures with nano- and/or submicro-array of particles.

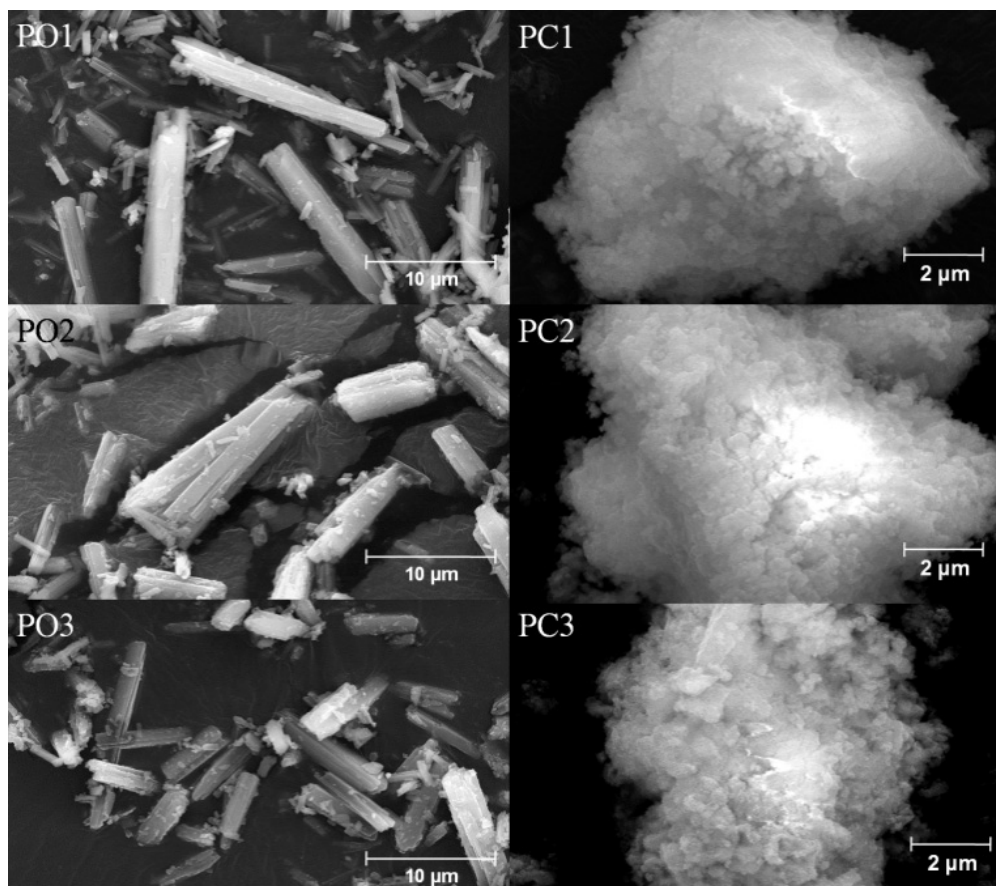


Figure 7. Morphologies of precursors.

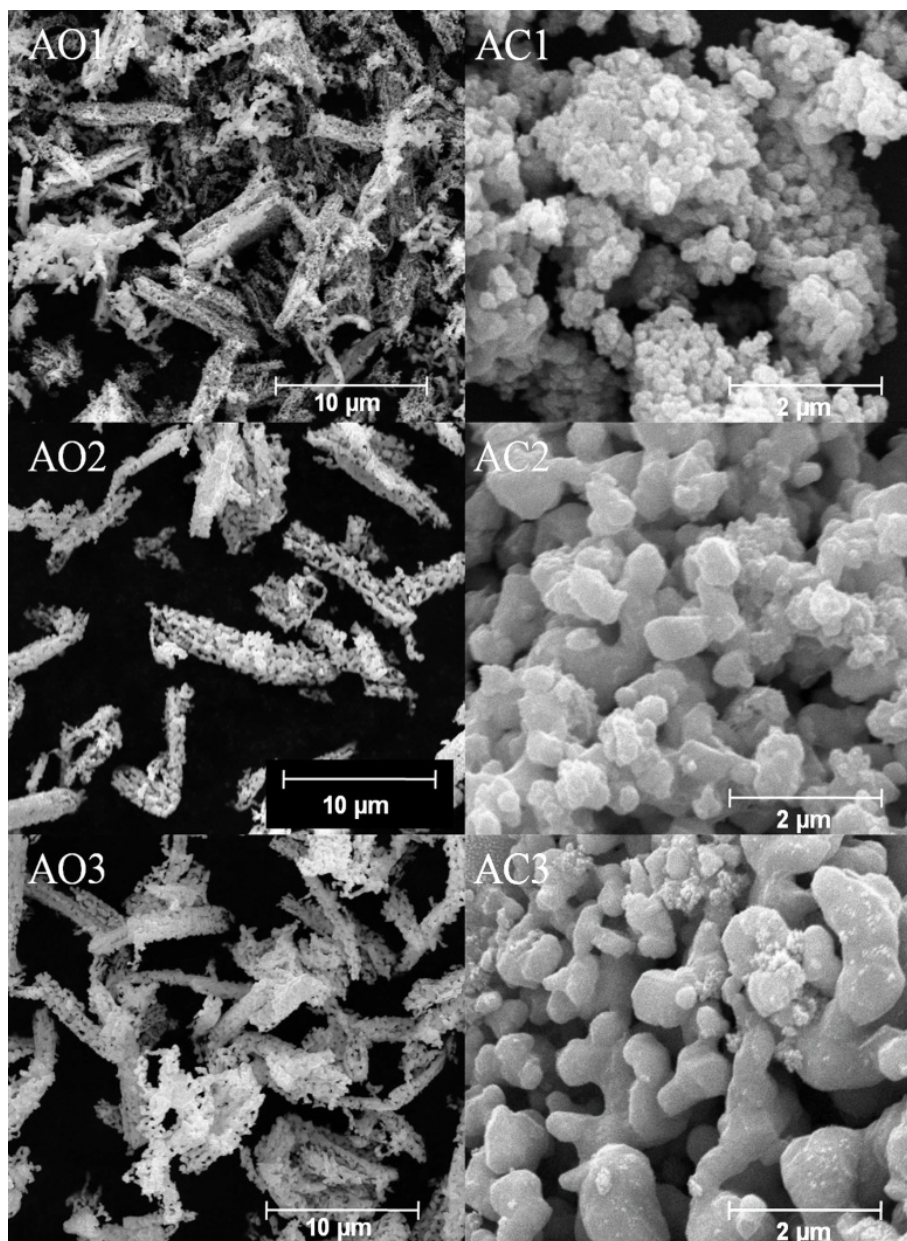


Figure 8. Morphologies of Co-Cr-V alloy powders.

It can be inferred that our Co-Cr-V alloy powders with rod-like morphologies have larger magneto-crystalline anisotropy and therefore larger coercivity compared to granular morphologies. In addition, it is known that coercivities of nanosized magnetic powders are proportional to the sixth power of their diameters [40]. In other words, with adjustable grain size (40–60 nm, see Section 3.1) and morphologies, the magnetic properties, especially coercivity, of nanosized Co-Cr-V alloy powders maybe tunable to satisfy different applications such as ultra-high density magnetic recording media and biomedical materials used in thermotherapy.

4. Conclusions

In conclusion, oxalate and basic carbonate precursors and Co-Cr-V alloy powders have been synthesized via coprecipitation method using $(\text{NH}_4)_2\text{C}_2\text{O}_4 \cdot \text{H}_2\text{O}$ and Na_2CO_3 as precipitants. Grain sizes of precursors and alloy powders were increased with pH and within nanosize ranges, due to equilibrium shift of $\text{C}_2\text{O}_4^{2-}$ or CO_3^{2-} inside their solutions, resulting in higher frequency of

collision among ions and larger potential difference between particles surfaces and diffuse layers. As-prepared Co-Cr-V alloy powders consisted of major fcc Co and minor hcp Co phases. The presence of fcc Co phase at room temperature could be ascribed to its containing nanosized grains less than 60 nm. Comparative analysis revealed that Na₂CO₃ is a more effective precipitant capable of generating higher yields of Co, Cr and V. Increase in pH value from 7 to 10 may favor coordination reactions rather than coprecipitation in solution, causing larger deviation of chemical composition of Co-Cr-V alloy powders from preset value. Rod-like particles and granular agglomerates were obtained for oxalate and basic carbonate precursors, respectively. Morphologies of Co-Cr-V alloy powders inherited from precursors were formed by loosely packed nano- and/or submicro-particles. With adjustable grain size and morphologies, these nanosized Co-Cr-V alloy powders could be used as promising catalytic, magnetic recording or structural materials.

Acknowledgments: The authors acknowledge partial support from the National High Technology Research and Development Program of China (2013AA032001) and Open Foundation of State Key Laboratory of Powder Metallurgy, Central South University.

Author Contributions: In this work, Xiaoyu Chen designed and conducted the experiments; Yongxia Li, Lan Huang, Dan Zou, Enxi Wu, Yanjun Liu and Yuanyan Xie provided reagents/materials/equipments; Rui Yao, Songyi Liao and Guangrong Wang helped for data analysis; Dr. Feng Zheng advised the entire work.

Conflicts of Interest: The authors declare no conflict of interest.

References

1. Knezevic, M.; Carpenter, J.S.; Lovato, M.L.; McCabe, R.J. Deformation behavior of the cobalt-based superalloy Haynes 25: Experimental characterization and crystal plasticity modeling. *Acta Mater.* **2014**, *63*, 162–168. [[CrossRef](#)]
2. Galerie, A. 1.23—High Temperature Corrosion of Chromia-forming Iron, Nickel and Cobalt-base Alloys. In *Shreir's Corrosion*; Richardson, T.J.A., Ed.; Elsevier: Oxford, UK, 2010; pp. 583–605.
3. Mori, M.; Yamanaka, K.; Sato, S.; Tsubaki, S.; Satoh, K.; Kumagai, M.; Imafuku, M.; Shobu, T.; Chiba, A. Strengthening of biomedical Ni-free Co-Cr-Mo alloy by multipass “low-strain-per-pass” thermomechanical processing. *Acta Biomater.* **2015**, *28*, 215–224. [[CrossRef](#)] [[PubMed](#)]
4. Liu, L.; Wu, S.; Yu, G.; Chen, Y. Oxidation behaviour and mechanism of a cobalt based superalloy between 1050 °C and 1250 °C. *Appl. Surf. Sci.* **2013**, *283*, 590–598. [[CrossRef](#)]
5. Aronson, J.K. (Ed.) *Meyler's Side Effects of Drugs*, 16th ed.; Elsevier: Oxford, UK, 2016; pp. 490–491.
6. Zhong, D.K.; Gamelin, D.R. Photoelectrochemical Water Oxidation by Cobalt Catalyst (“Co-Pi”)/α-Fe₂O₃ Composite Photoanodes: Oxygen Evolution and Resolution of a Kinetic Bottleneck. *J. Am. Chem. Soc.* **2010**, *132*, 4202–4207. [[CrossRef](#)] [[PubMed](#)]
7. Ye, W.; Zhang, H.; Xu, D.; Ma, L.; Yi, B. Hydrogen generation utilizing alkaline sodium borohydride solution and supported cobalt catalyst. *J. Power Sources* **2007**, *164*, 544–548. [[CrossRef](#)]
8. Lu, X.B.; Darensbourg, D.J. Cobalt catalysts for the coupling of CO₂ and epoxides to provide polycarbonates and cyclic carbonates. *Chem. Soc. Rev.* **2012**, *41*, 1462–1484. [[CrossRef](#)] [[PubMed](#)]
9. Panpranot, J.; Kaewkun, S.; Praserttham, P.; Goodwin, J.G. Effect of Cobalt Precursors on the Dispersion of Cobalt on MCM-41. *Catal. Lett.* **2003**, *91*, 95–102. [[CrossRef](#)]
10. Xi, X.; Nie, Z.; Jiang, Y.; Xu, X.; Zuo, T. Preparation and characterization of ultrafine cobalt powders and supported cobalt catalysts by freeze-drying. *Powder Technol.* **2009**, *191*, 107–110. [[CrossRef](#)]
11. Klarstrom, D.; Crook, P.; Mridha, S. Cobalt Alloys: Alloy Designation System. In *Reference Module in Materials Science and Materials Engineering*; Elsevier: Oxford, UK, 2016; pp. 1279–1280.
12. Plumer, M.L.; Ek, J.V.; Weller, D. (Eds.) *The Physics of Ultra-High-Density Magnetic Recording, the Physics of Ultra-High-Density Magnetic Recording*; Springer: Berlin, Germany, 2001; pp. 1–32.
13. Vajpai, S.K.; Sawangrat, C.; Yamaguchi, O.; Ciuca, O.P.; Ameyama, K. Effect of bimodal harmonic structure design on the deformation behaviour and mechanical properties of Co-Cr-Mo alloy. *Mater. Sci. Eng. C* **2016**, *58*, 1008–1015. [[CrossRef](#)] [[PubMed](#)]
14. Okamoto, H. Co-V (Cobalt-Vanadium). *J. Phase Equilib. Diffus.* **2007**, *28*, 314. [[CrossRef](#)]

15. Zhao, C.; Yu, Y.; Liu, X.; Wang, C.P. Experimental determination of phase equilibria in the Co-Cr-V ternary system. *J. Phase Equilib. Diffus.* **2012**, *33*, 189–194. [[CrossRef](#)]
16. Qin, D.; Wang, C.; Sun, Q.; Li, H.L. The effects of annealing on the structure and magnetic properties of CoNi patterned nanowire arrays. *Appl. Phys. A* **2002**, *74*, 761–765. [[CrossRef](#)]
17. Thongmee, S.; Pang, H.; Yi, J.; Ding, J.; Lin, J.Y.; Van, L.H. Unique nanostructures in NiCo alloy nanowires. *Acta Mater.* **2009**, *57*, 2482–2487. [[CrossRef](#)]
18. Li, X.Z.; Wei, X.W.; Ye, Y. Template electrodeposition to cobalt-based alloys nanotube arrays. *Mater. Lett.* **2009**, *63*, 578–580. [[CrossRef](#)]
19. Vahid, S.; Mirzaei, A.A. An investigation of the kinetics and mechanism of Fischer-Tropsch synthesis on Fe-Co-Ni supported catalyst. *J. Ind. Eng. Chem.* **2014**, *20*, 2166–2173. [[CrossRef](#)]
20. Wu, K.-L.; Wei, X.-W.; Zhou, X.-M.; Wu, D.-H.; Liu, X.-W.; Ye, Y.; Wang, Q. NiCo₂ alloys: Controllable synthesis, magnetic properties, and catalytic applications in reduction of 4-nitrophenol. *J. Phys. Chem. C* **2011**, *115*, 16268–16274. [[CrossRef](#)]
21. Zhu, L.P.; Xiao, H.M.; Fu, S.Y. Surfactant-Assisted Synthesis and Characterization of Novel Chain-Like CoNi Alloy Assemblies. *Eur. J. Inorg. Chem.* **2007**, *25*, 3947–3951. [[CrossRef](#)]
22. Ung, D.; Viau, G.; Ricolleau, C.; Warmont, F.; Gredin, P.; Fiévet, F. CoNi nanowires synthesized by heterogeneous nucleation in liquid polyol. *Adv. Mater.* **2005**, *17*, 338–344. [[CrossRef](#)]
23. Wen, M.; Wang, Y.F.; Zhang, F.; Wu, Q.S. Nanostructures of Ni and NiCo amorphous alloys synthesized by a double composite template approach. *J. Phys. Chem. C* **2009**, *113*, 5960–5966. [[CrossRef](#)]
24. Domínguez-Crespo, M.; Plata-Torres, M.; Torres-Huerta, A.; Arce-Estrada, E.M.; Hallen-Lopez, J.M. Kinetic study of hydrogen evolution reaction on Ni₃₀Mo₇₀, Co₃₀Mo₇₀, Co₃₀Ni₇₀ and Co₁₀Ni₂₀ Mo₇₀ alloy electrodes. *Mater. Charact.* **2005**, *55*, 83–91. [[CrossRef](#)]
25. Bahlawane, N.; Premkumar, P.A.; Tian, Z.Y.; Hong, X.; Qi, F.; Kohse-Höinghaus, K. Nickel and nickel-based nanoalloy thin films from alcohol-assisted chemical vapor deposition. *Chem. Mater.* **2009**, *22*, 92–100. [[CrossRef](#)]
26. Chow, G.; Ding, J.; Zhang, J.; Lee, K.Y.; Surani, D. Magnetic and hardness properties of nanostructured Ni-Co films deposited by a nonaqueous electroless method. *Appl. Phys. Lett.* **1999**, *74*, 1889–1891. [[CrossRef](#)]
27. Behrens, M. Coprecipitation: An excellent tool for the synthesis of supported metal catalysts—from the understanding of the well known recipes to new materials. *Catal. Today* **2015**, *246*, 46–54. [[CrossRef](#)]
28. Buschow, K.H.J. *Handbook of Magnetic Materials*; Elsevier: Oxford, UK, 2003.
29. Noce, R.D.; Barelli, N.; Sumodjo, P.T.A.; Comejo, D.R.; Benedetti, A.V. Effect of the bath pH on the electrodeposition of nanocrystalline Pd-Co alloys and their magnetic properties. *J. Magn. Magn. Mater.* **2006**, *306*, 199–203. [[CrossRef](#)]
30. Wu, K.H.; Huang, W.C.; Wang, G.P.; Wu, T.R. Effect of pH on the magnetic and dielectric properties of SiO₂/NiZn ferrite nanocomposites. *Mater. Res. Bull.* **2005**, *40*, 1822–1831. [[CrossRef](#)]
31. Wu, Z.; Zhou, W.; Jin, W.; Xu, N. Effect of pH on synthesis and properties of perovskite oxide via a citrate process. *AIChE J.* **2006**, *52*, 769–776. [[CrossRef](#)]
32. Thu, T.N.T.; Thi, N.N.; Quang, V.T.; Hong, K.N.; Minh, T.N.; Hoai, N.L.T. Synthesis, characterisation, and effect of pH on degradation of dyes of copper-doped TiO₂. *J. Exp. Nanosci.* **2016**, *11*, 226–238.
33. Rong, Y. Phase transformations and phase stability in nanocrystalline materials. *Curr. Opin. Solid State Mater. Sci.* **2005**, *9*, 287–295. [[CrossRef](#)]
34. Zhao, X.; Veintemillas-Verdaguer, S.; Bomati-Miguel, O.; Morales, M.P.; Xu, H.B. Thermal history dependence of the crystal structure of Co fine particles. *Phys. Rev. B* **2005**, *71*. [[CrossRef](#)]
35. Kitakami, O.; Sato, H.; Shimada, Y.; Sato, F.; Tanaka, M. Size effect on the crystal phase of cobalt fine particles. *Phys. Rev. B* **1997**, *56*, 13849–13854. [[CrossRef](#)]
36. Meng, Q.P.; Rong, Y.H.; Xu, Y.Z. The structural stability in nano-sized crystals of metals. *Sci. China Ser. E Technol. Sci.* **2002**, *45*, 485–494.
37. Jing, Z.; He, Y.H.; Zhou, D.F.; Zhang, C.F. Thermodynamic analysis on synthesis of fibrous Ni-Co alloys precursor and Ni/Co ratio control. *Trans. Nonferr. Met. Soc. China* **2011**, *21*, 1141–1148.
38. Jongen, N.; Bowen, P.; Lemaître, J.; Valmalette, J.C.; Hofmann, H. Precipitation of self-organized copper oxalate polycrystalline particles in the presence of hydroxypropylmethylcellulose (HPMC): Control of Morphology. *J. Colloid Interface Sci.* **2000**, *226*, 189–198. [[CrossRef](#)]

39. Zhan, J.; Zhou, D.F.; Zhang, C.F. Shape-controlled synthesis of novel precursor for fibrous Ni-Co alloy powders. *Trans. Nonferrous Met. Soc. China* **2011**, *21*, 544–551. [[CrossRef](#)]
40. Callister, W.D.; Rethwisch, D.G. *Materials Science and Engineering: An Introduction*, 7th ed.; Wiley: New York, NY, USA, 2007.



© 2017 by the authors. Licensee MDPI, Basel, Switzerland. This article is an open access article distributed under the terms and conditions of the Creative Commons Attribution (CC BY) license (<http://creativecommons.org/licenses/by/4.0/>).